

*Optical Modeling and Analysis of a High Throughput and High Temporal Resolution  
Spectrometer*

**Raz Rivlis**

Brighton High School

Rochester, New York

Adviser: Robert Boni

**Laboratory for Laser Energetics**

University of Rochester

Rochester, New York

Summer, 2012

## ***1. Abstract***

A newly designed UV spectrometer will replace the current 351 nm, full aperture backscatter (FABS) spectrometer that is used in the OMEGA laser system. The FABS spectrometer has a time resolution of 270 ps. The new spectrometer will improve the temporal resolution to 10 ps, while maintaining signal throughput by superimposing 27 separate spectra onto the detector. This is accomplished by placing a 27-element roof mirror array between two identical diffraction gratings operating at opposite orders. The retro-reflecting property of the roof mirror array breaks the 270 ps pulse front tilt into 27 10 ps pulse front tilts. FRED, an optical design program, was used to model the spectrometer. Image rotation, pulse front tilt, and images from other grating orders were analyzed. It was found that image rotation can be corrected by rotating the input slit. The separation between the roof mirror array and the gratings was chosen to prevent images from other grating orders from reaching the detector. The pulse front tilt analysis demonstrates that the spectrometer will achieve the desired 10 ps time resolution.

## ***2. Introduction***

The OMEGA laser system is used to study the direct drive approach to inertial confinement fusion. In the OMEGA system, a FABS spectrometer collects 351 nm light that scatters back into the laser path.<sup>1</sup> The spectrometer, coupled to a streak camera, is used to measure the spectral shift of the backscattered light as a function of time, giving information on the evolution of a target irradiated by the OMEGA laser.<sup>1,2,3</sup> The current spectrometer has a time resolution of 270 ps, but by masking 2/3 of the light, the temporal resolution is reduced to 90 ps. Our goal is to obtain better time resolution, without sacrificing throughput.

When using a single grating, throughput and time resolution are linked. Improving time resolution generally requires masking the grating, which reduces throughput, as shown in Figure 1. When light reflects off a grating, the angle of the reflected light differs from that of the incident light. This causes a delay between two light paths separated in space due to a difference in path length.

To increase the throughput, while maintaining resolving power and time resolution, one possible solution is to operate multiple spectrometers in parallel as shown in Figure 2. The input is an f/4 fiber optic cable. To obtain the desired time resolution, we could mask the input down to f/108. If we could instead split the input into 27 f/108 sections, we would lose no light from the input, and we would obtain the desired time resolution. The total throughput is the sum of those from each of the individual spectrometers. However, building such a spectrometer would be highly impractical, as it would require alignment of a huge number of small optical elements.

Instead, we explore a method to break up the pulse front tilt, effectively creating multiple spectrometers in parallel.

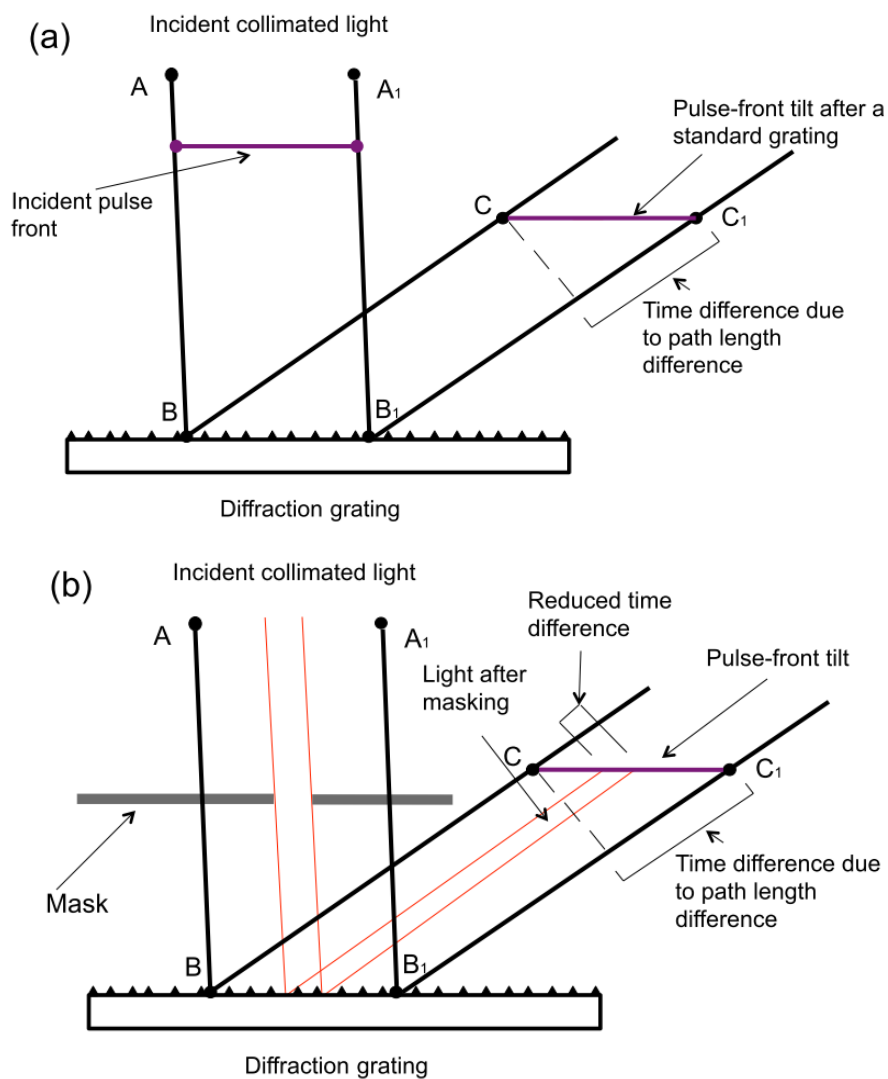


**Figure 1:**

(a) A standard spectrometer, with a large pulse front tilt and a large throughput. The output light is focused by lenses (not shown) to separate the different wavelengths in the incident beam.

(b) The same spectrometer, masked to reduce pulse front tilt. This also reduces the throughput.

### 3. Design of Spectrometer

In this section we describe how a roof mirror array can be used to improve time resolution of the spectrometer, without sacrificing throughput. The concept was originated by R. Boni.<sup>4</sup>

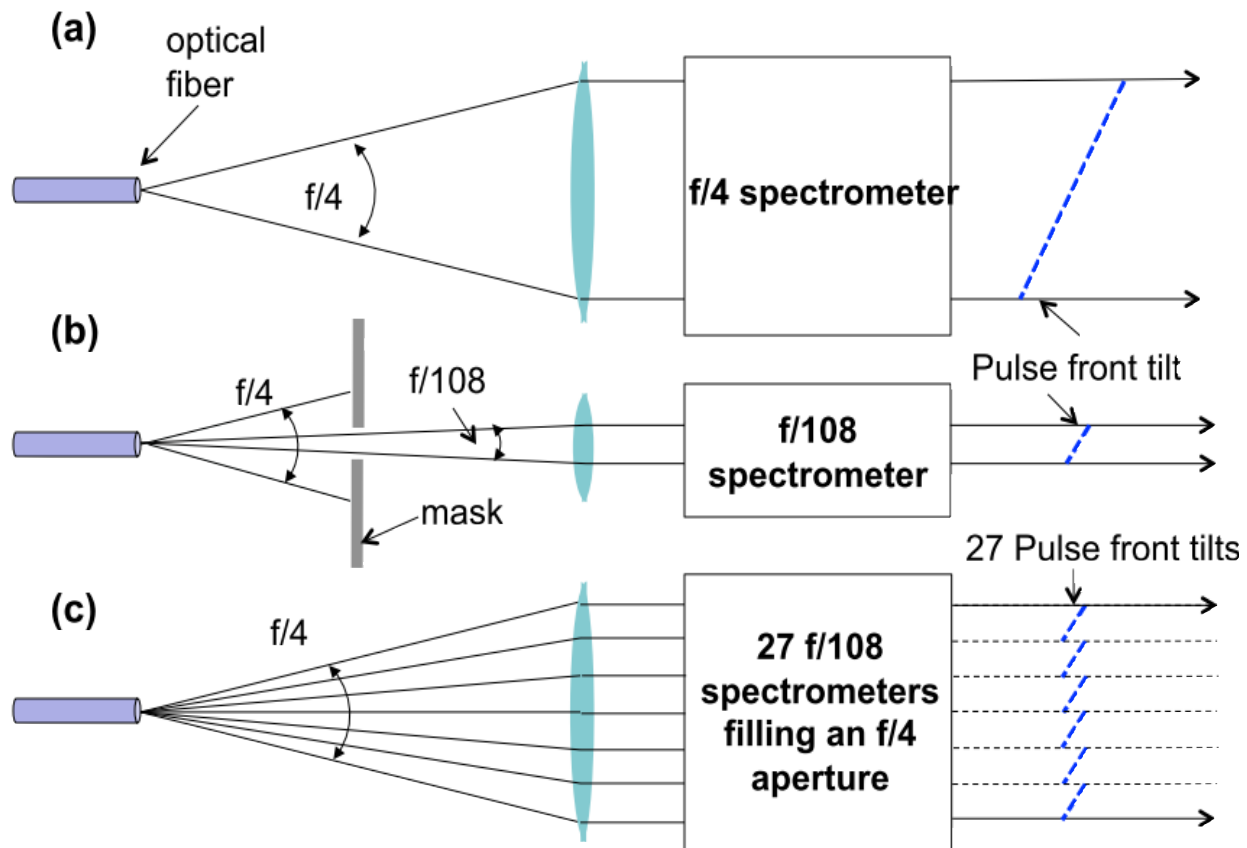


**Figure 2:** (a) A standard  $f/4$  spectrometer with a large throughput and large pulse front tilt. (b) An  $f/108$  spectrometer with a small pulse front tilt and small throughput. (c) 27  $f/108$  spectrometers used in parallel to fill an  $f/4$  cone, resulting in a high throughput and high time resolution.

### 3.1 Use of a roof mirror array to improve time resolution

A roof mirror is two mirrors oriented 90 degrees from each other. A roof mirror array is a series of roof mirrors, as shown in Figure 3. While roof mirrors are not uncommonly used, roof mirror arrays have never been built to optical quality. Placing a roof mirror array between two diffraction gratings operating at opposite orders causes the pulse front tilt to segment. As shown in Figure 3, the roof mirror segments the pulse front tilt from the first grating by flipping each segment of the reflected pulse front tilt. However, there is still a

large overall pulse front tilt. The second grating removes this, but keeps the small segments, creating multiple small pulse front tilts. This improves the total time resolution, while preserving the throughput of the incoming light.

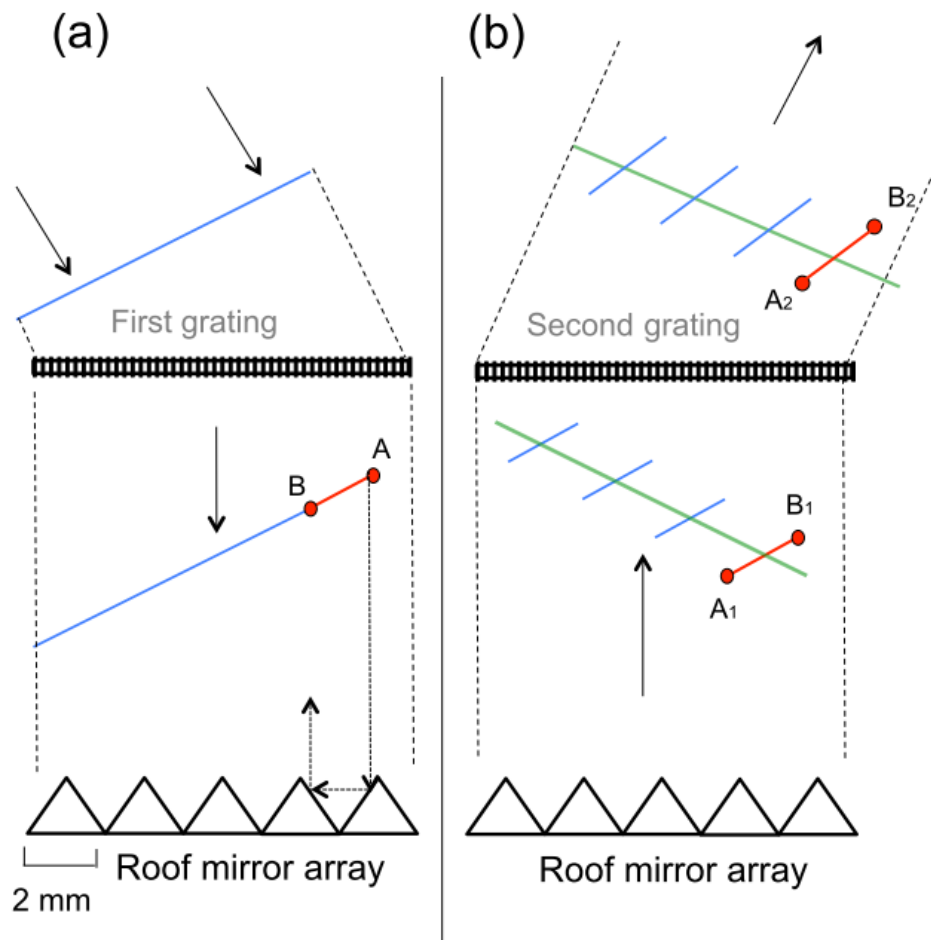


**Figure 3:** This schematic illustrates the use of a roof mirror array between two gratings to reduce the pulse front tilt. Gratings are drawn as transmission gratings to aid visualization. Each point A corresponds to the same ray, as does each point B. (a) Incoming light passes through the first grating, creating a large pulse front tilt. (b) The pulse front tilt is segmented by the roof mirror array. The green line would be the reflection off an ordinary mirror. The large pulse front tilt is canceled out by the second grating, operating at opposite order from the first one. The tilt for each segment is doubled as it passes through the second grating.

### 3.2 Choice of Grating Order to Improve Efficiency

We will operate the gratings at plus and minus 7th order. By operating the gratings at 7th order we can use a grating with wide groove spacings. This is seen from the grating equation:

$$n\lambda = d(\sin\alpha + \sin\beta) \quad (1)$$

where  $n$  is the order,  $\lambda$  is the wavelength of light,  $d$  is the distance between grooves,  $\alpha$  is the incident angle, and  $\beta$  is the resultant angle.<sup>5</sup> For fixed incident and resultant angles, larger  $d$  corresponds to larger  $n$ . Increasing the groove spacing is desirable because it increases efficiency. Efficiency is reduced when the groove spacing approaches the wavelength of light because p-polarized light experiences edge effects. This is shown in Figure 4. The drawback to operating at high orders is that it causes nearby orders to be closer to the desired order. This increases the risk that nearby orders are imaged on the detector. This problem is examined below.

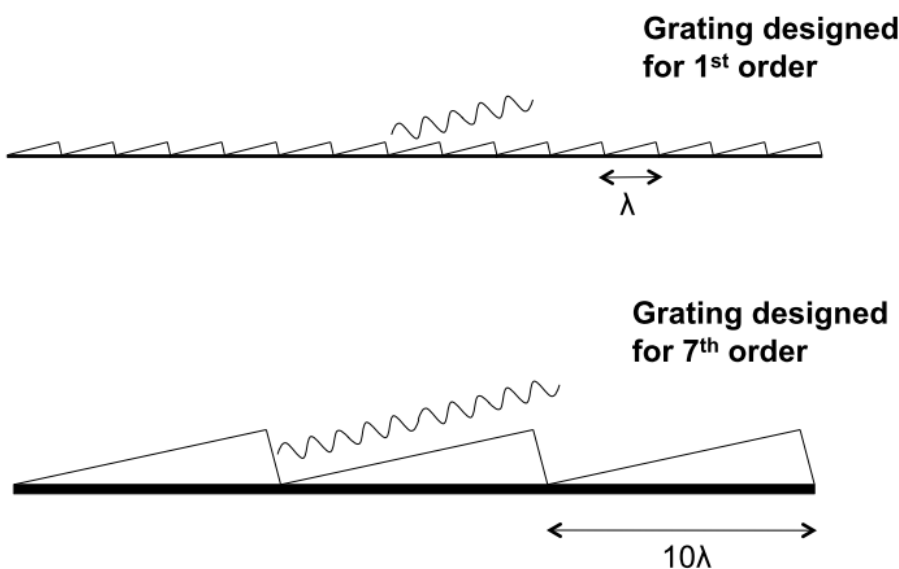


**Figure 4:** This shows how the groove spacing approaches the wavelength of light ( $\lambda$ ) at 1st order, but not 7th. This causes loss of light from p-polarization due to edge effects. S-polarized light is unaffected because its polarization follows the long axis of the grooves.

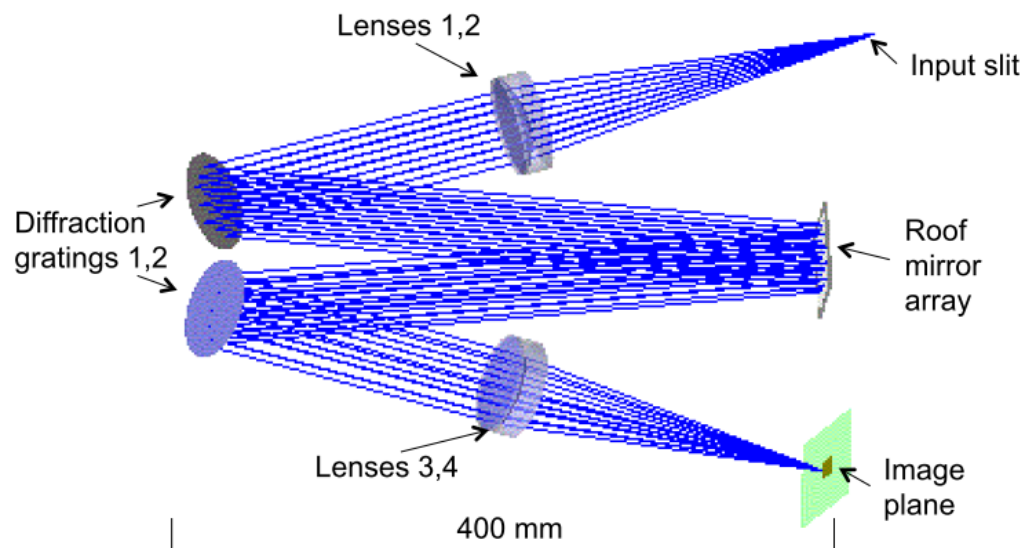
### 3.3 Initial Design

The initial design was done by R. Boni,<sup>4</sup> using OSLO, an optical modeling software. OSLO was used to optimize the lens placement to achieve the smallest spot size in the image plane. However, OSLO was unable to check the temporal resolution, image rotation, and order crosstalk.

### 4. *Optical Modeling*

The spectrometer design was analyzed using FRED Optical Engineering Software, developed by Photon Engineering,<sup>6</sup> that simulates the propagation of light through an optical system by raytracing. FRED allows the user to control the light source, scattering, and grating orders. We used FRED to model a slit input source, model multiple grating orders, measure image rotation, and determine the pulse-front tilt.

Figure 5 shows the optical layout and the ray path at 7th order. The detector we are using is a ROSS streak camera, and it will be located at the image plane. The streak camera will record a one dimensional slit over time, with high temporal resolution. The ray path shown in Figure 5 does not lie in a single plane. This is because the roof mirror array is a one dimensional retro mirror, and if the ray path was not taken out of plane, the gratings would have to lie in the same physical space. Tables 1 and 2 list properties of the optical elements. Both Table 1 and Figure 5 show the final design resulting from this work. The primary modification to the initial design is the roof mirror to grating distance as discussed in Section 4.4. In Table 1, the distance to the next element is measured along the ray path. Because the spectrometer operates near 351 nm, CaF<sub>2</sub> and fused silica lenses are used for their high UV transmittance.

**Figure 5:**

Raytrace diagram as modeled by FRED.

Note that the ray path does not travel in a single plane.

**Table 1: Optical elements of the spectrometer:** The radii of curvature for each element are listed along with its material and the distance to the next element along the ray path.

Optic	Front Radius of Curvature (mm)	Back Radius of Curvature (mm)	Thickness (mm)	Aperture (mm)	Material	Distance to next element (mm)
Lens 1	291	59.6	8	35	Fused Silica	.072
Lens 2	59.6	-145	18	35	CaF <sub>2</sub>	200
Grating 1	-	-	-	36	-	400
Roof Mirror	-	-	-	27 by 30	-	400
Grating 2	-	-	-	36	-	200
Lens 3	-145	59.6	18	35	CaF <sub>2</sub>	.072
Lens 4	59.6	291	8	35	Fused Silica	227

**Table 2: Tilt of the elements, relative to the previous element along the ray path:** At the input slit, the Z direction is along the ray path, X is arbitrarily chosen, and Y is perpendicular to X and Z.

Optic	Tilts
Grating 1	11.37° X tilt, 6° Y tilt
Roof Mirror Array	-6° Y tilt
Grating 2	-32.68° X tilt, 6° Y tilt

#### 4.1 Image rotation

The FRED model showed that the spectrometer rotated the image as shown in Figure 6(a). This rotation occurred because the ray path was out of plane, and some elements are tilted around both X and Y axes (see Figure 5 and Table 2). The streak camera window is approximately 0.2 mm. This rotation seen in Figure 6(a), over the width of the window, which is in the x axis in the figure, causes the spectrum to blur by around 0.05 nm. The streak camera records only one spatial dimension, so all horizontal information is lost. The rotation cannot be removed by rotating the detector, because we would not detect the light at the edges of our desired frequency range. The bands would no longer be rotated or blurred, but the edges of the spectrum would fall outside the window. The rotation can be corrected by rotating the input slit instead. We used the FRED model, as shown in Figure 6(b), to determine that the input slit must be rotated 7.5° in the opposite direction to the rotation to remove it. This value was determined by trying a few different values and minimizing the modeled image rotation.

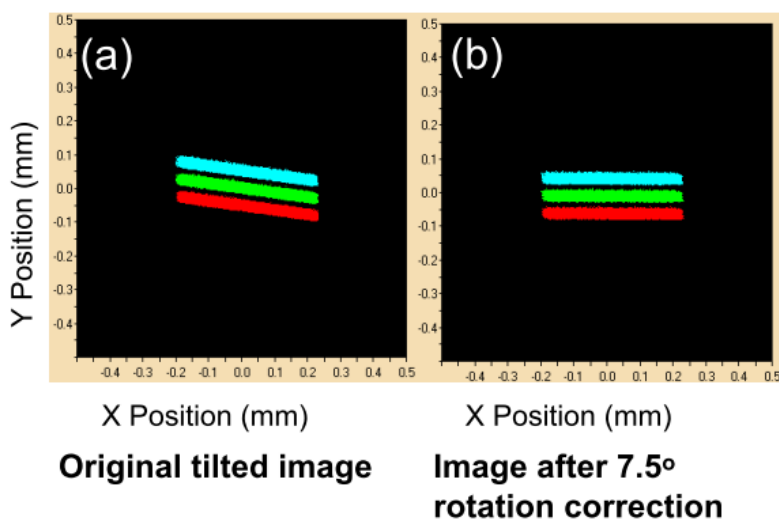


**Figure 6:** (a) Spot diagram at the image plane. Note that each color rotates individually. (b) Spot diagram at the detector after the input slit has been rotated 7.5°.

Red = 351.05 nm light  
 Green = 351 nm light  
 Blue = 350.95 nm light

#### 4.2 Spatial resolution and resolving power at 7th order

FRED was used to model the spatial resolution and resolving power. Using a spot diagram at the image plane, where the detector will be located, we determined that the spectrometer has a spatial resolution of 50 microns, and a resolving power of 0.05 nm. This means that the spectrometer will detect wavelengths 0.05 nm apart, and will image them 50 microns apart. Figure 7 is an expanded view of Figure 6(b). The figure suggests that we could detect a smaller wavelength difference; however, we lose some resolution from the streak camera. The streak camera's pixel size is 50 microns, so the spectrometer creates no additional loss of resolution. This model is consistent with the OLSO model. However, the FRED model is more accurate, because it takes into account rays from the entire input slit. OSLO can only model point sources.

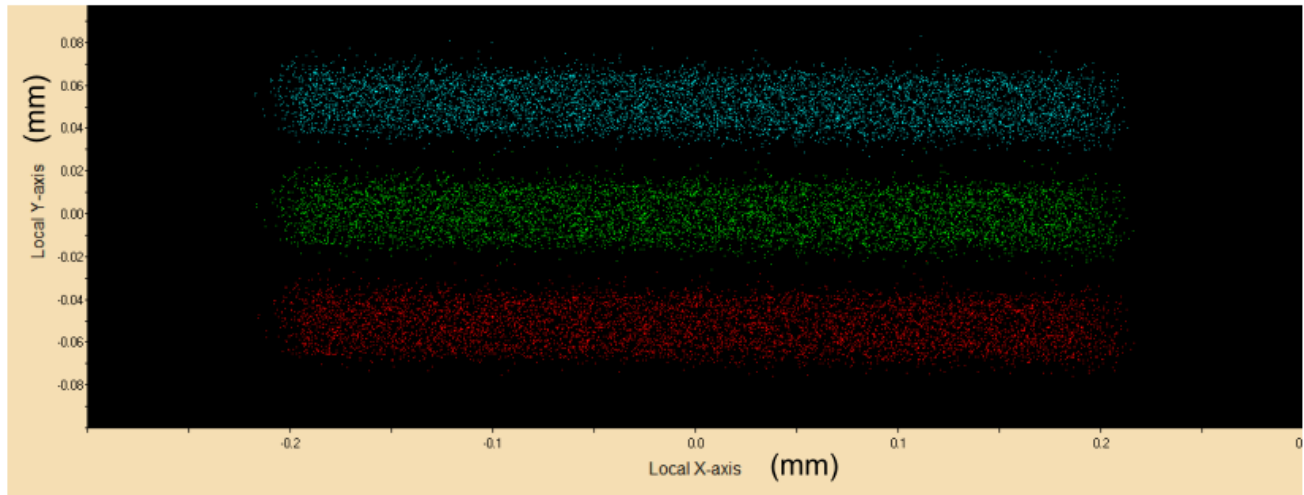


**Figure 7:** Spot diagram from the spectrometer at the image plane. Red spots are light at 351.05 nm, green at 351 nm, blue at 350.95 nm. Along the Y axis, there are 50 microns of dispersion between each band of light. The spot width is 40 microns.

### 4.3 Temporal resolution

Most spectrometers do not need to operate at high temporal resolution, so raytracing software is not designed to measure pulse front tilt. However, the FRED model can be used to determine the physical path length of each ray. From this we can calculate the pulse front tilt. We measured the physical path length from the source to a plane right before refocusing (right before lens 3; see Figure 5). We recorded the X and Y position of each ray at the final plane. We normalized all these distances, so that we had the difference in X, Y, and path length. We then converted the path length difference to a time difference. Next, we used Matlab to make a plot of time delay vs. position in the column of light, as shown in Figure 8. This plot clearly shows how multiple pulse front tilts are created by the roof mirror array. Furthermore, the model output verified that we obtained the desired time resolution of 10 ps.

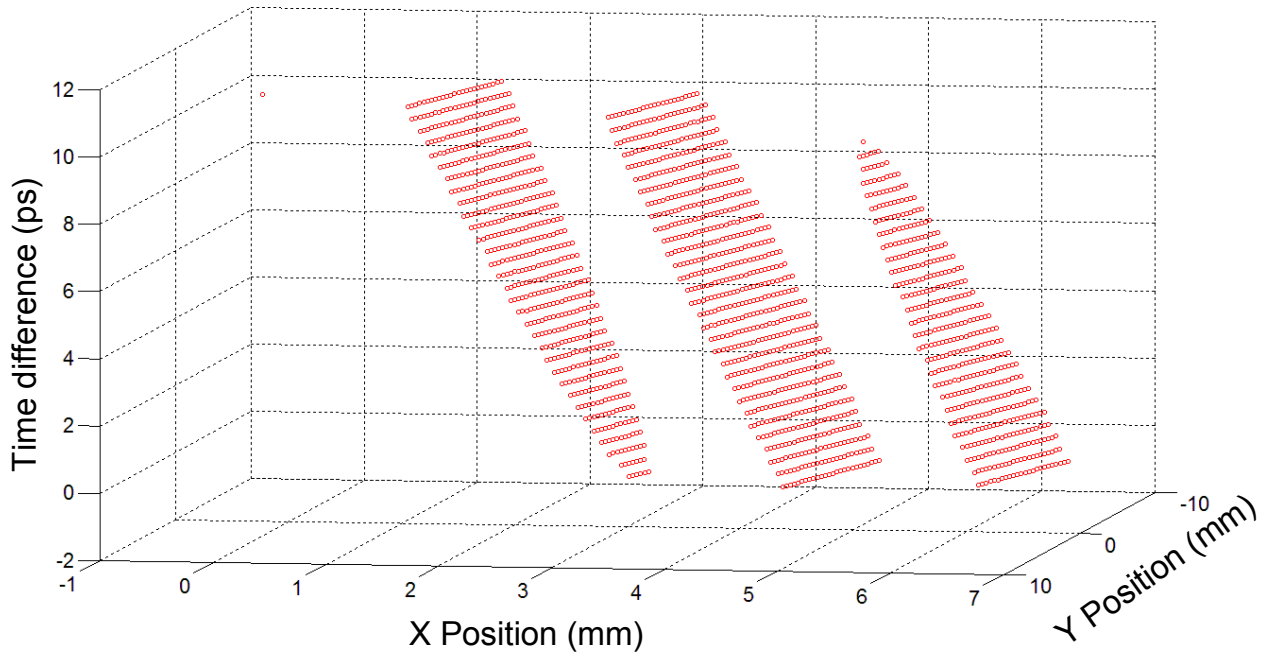


**Figure 8:** Plot of time difference against position in the column of light. Because this plot only shows 3 of the 27 pulse front tilts, and is not in the focal plane, three groups are seen. Note that each of these pulse front tilts is only 10 ps wide, as seen on the Z axis. The model successfully shows each individual pulse front tilt.

#### 4.4 Order crosstalk

A problem that must be considered is the risk of nearby orders imaging onto the detector, known as crosstalk between orders. Figure 9 shows the initial FRED model, taking into account 6th, 7th, and 8th orders. To completely examine this problem, we calculated the resultant angles and linear displacement for all orders from both gratings between  $n = 0$  and 9. We used the following variations on the grating equation (Equation 1),

$$\beta_1 = \text{asin}(n_1\lambda/d - \sin\alpha_1) \quad (2)$$

$$\alpha_2 = \beta_1 + 65.38^\circ \quad (3)$$

$$\beta_2 = \text{asin}(n_2\lambda/d - \sin\alpha_2) \quad (4)$$

where  $\alpha_1$  is the incident angle on the first grating,  $\alpha_2$  is the incident angle on the second grating,  $\beta_1$  is the resultant angle from the first grating,  $\beta_2$  is the resultant angle from the second grating,  $n_1$  is the first grating order,  $n_2$  is the second grating order,  $d$  is the groove spacing, and  $\lambda$  is the wavelength. Our wavelength is always 0.351 micrometers,  $\alpha_1$  is always  $11.37^\circ$  and  $d$  is always 1/300 mm. The conversion from  $\beta_1$  to  $\alpha_2$  comes from the physical layout of the spectrometer;  $65.36^\circ$  is the angle between the 2 gratings. This is calculated from the angles in Table 2 and is equal to  $32.68 \times 2$ . Using these three equations, we calculated the resultant angle for the different order combinations. We then subtracted  $11.37^\circ$  from each resultant angle, giving us the angle to the center of the detector plane. We took the tangent of the resultant angle and multiplied by the focal length of the second lens system to determine the location of the image on the detector.

We considered two criteria for significant order problems: the resultant distance was close to the desired image, and the ray path intersected the roof mirror array. There were only four significant order combinations that are potentially a problem and these are listed in Table 3. We used our FRED model to predict the locations and intensities of these problematic orders in the image plane, and these are shown in Figure 10. Our computations of the image locations (in Table 3) agree with those computed using the FRED ray tracing model.

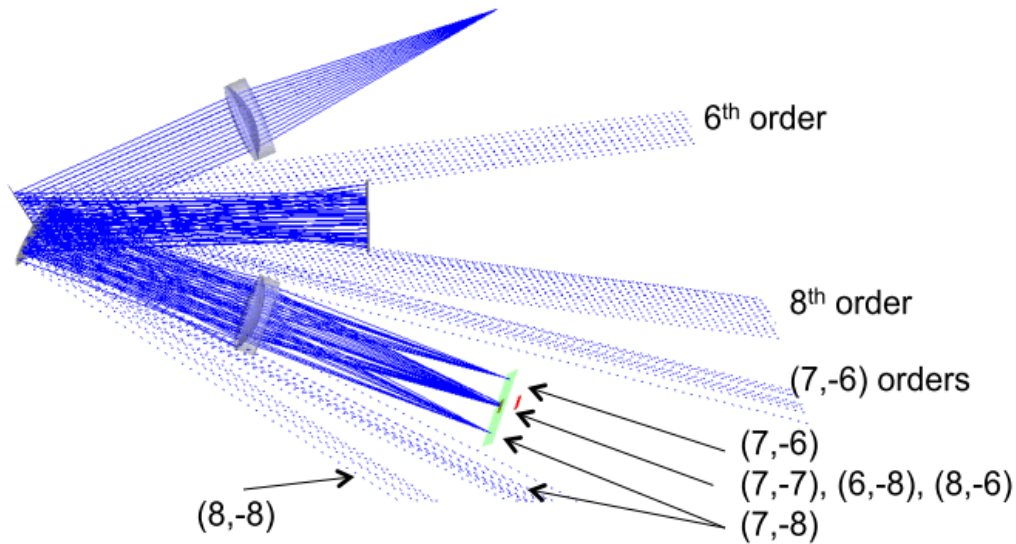


**Figure 9:** Raytracing showing the various order combinations that could cause order crosstalk. The center spot on the image plane is three spots caused by three different order combinations. The detector lies in the green plane, but is smaller. The (7, -6) and (7, -8) orders do not intersect the detector.

**Table 3: Location of images from contaminating orders:** Distance of image, in the image plane, from the 7th order image for nearby grating orders, in mm. These distances were calculated using Equations 2, 3, and 4.

Order of First grating	Order of Second Grating		
	-6	-7	-8
6			2.15
7	-24.23	0	24.76
8	1.83		

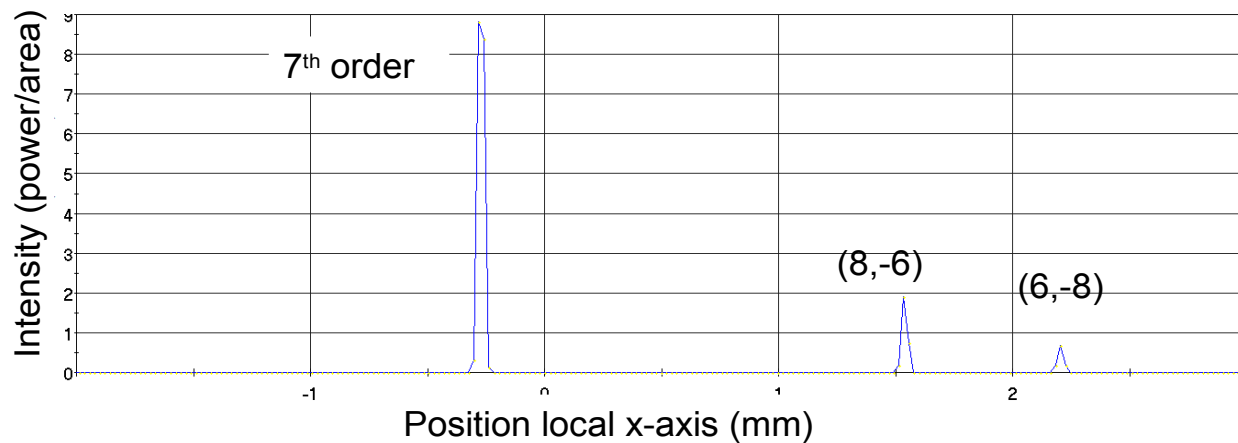


**Figure 10:** This graph plots light intensity (y axis) vs. position of focal plane (x axis) in mm, computed in FRED. The image near  $x = 0$  is the 7th order image. The other two images correspond to the (6, -8) and (8, -6) order images as shown in Table 3.

To eliminate the (6, -8), and (8, -6) orders, we modified the design so fewer rays from these orders intersect the roof mirror array. We did this by moving the roof mirror array from 300 mm, where it originally was, to 400 mm. If we moved the roof mirror array back further, even fewer rays would intersect it, but the spectrometer would become bigger and more awkward to build and use in the OMEGA target bay. Figure 11 shows the 6th and 8th order paths missing the roof mirror. We ran a FRED model that takes into account the efficiencies of the gratings to estimate the intensity of the brightest undesired order image. We find that with the new design, the brightest undesired order is a factor of 100 below the primary image, as seen in Figure 12. An image that dim would not be detected, and so is irrelevant.

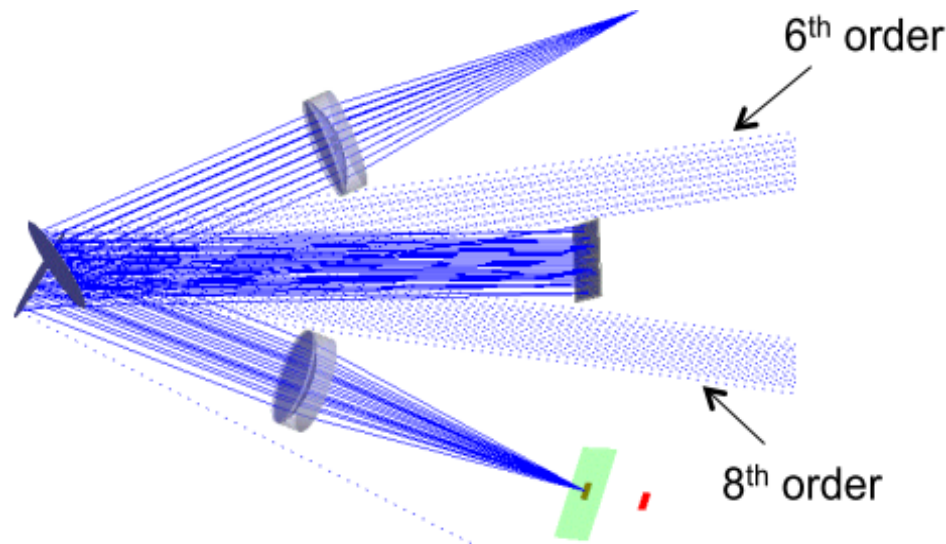


**Figure 11:** Raytracing showing 6th and 8th orders missing the roof mirror, after increasing the roof mirror-grating distance.

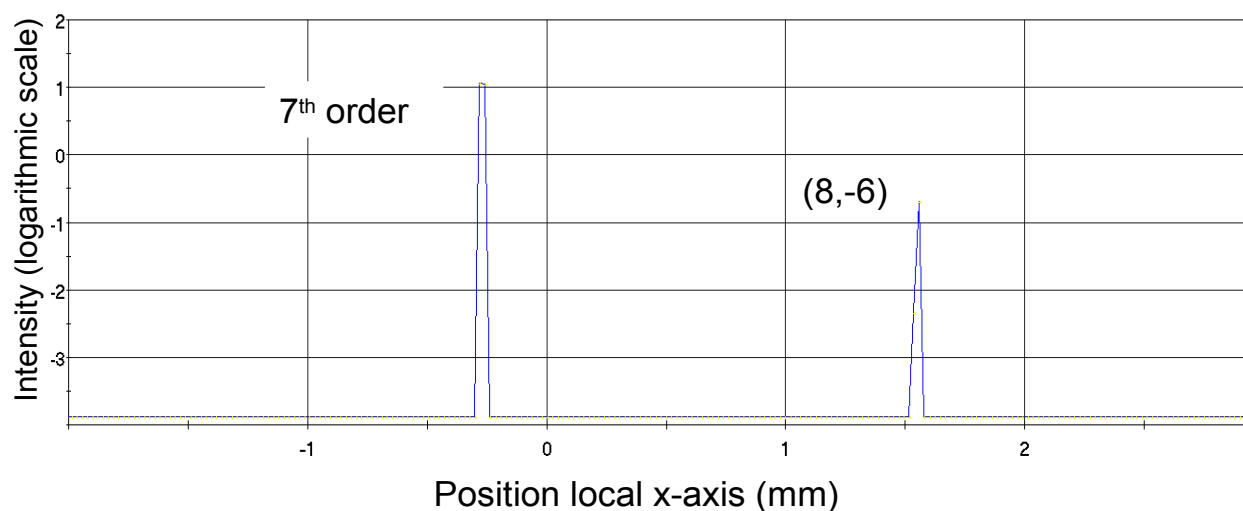


**Figure 12:** Intensity vs. X-axis position, The image near  $x = 0$  is the 7th order image. The other image corresponds to the (8, -6) order image. Note that this image is 2 decades dimmer than the desired image.

The other two order combinations that could be problematic are the (7, -6) and (7, -8) orders (shown in Table 3). These cannot be removed by moving the roof mirror array, as their rays follow the same path as the desired image until the second grating. However, they do not actually image on the detector (see Figure 9). They image near the detector instead. This means that they will only become a problem if light of other frequencies enters the spectrometer. We

determined using FRED that light more than 30 nm from the central wavelength will image onto the detector. To avoid this, we will add a 30 nm bandpass filter, centered on 351 nm. This filter will remove these undesired orders.

### ***5. Summary and Future Work***

We have designed a spectrometer that drastically improves temporal resolution, while preserving throughput. This spectrometer will replace the 351 nm backscatter spectrometer in the OMEGA system, and will improve the temporal resolution by a factor of 9, to 10 ps, and the throughput by a factor of 3. The design was modeled using FRED, and shows that a roof mirror array between two gratings is an effective way to reduce pulse front tilt. We discovered that the input slit must be rotated  $7.5^\circ$  to align the image with the streak camera window. The location of the roof mirror array was moved to remove an undesired order. It will be located 400 mm from the gratings. A 30 nm bandpass filter to remove other undesired orders.

The current spectrometer is used to study plasma instabilities that prevent high efficiency compression of the target and absorption of laser light in direct drive inertial confinement fusion experiments.<sup>2,7,8</sup> Efficient fusion will not be achieved if these instabilities prevent compression of the fuel. When ion-acoustic waves (sound waves in a plasma) are excited by laser light, they evolve on a time scale of 10 ps. Current diagnostics cannot achieve this resolution.<sup>8</sup> Temporally resolving the scattered light will allow us to measure the temporal evolution of the ion-acoustic waves, allowing us to design experiments with higher efficiency compression. Very few measurements have been made of this ion-acoustic wave scattering process at this resolution.

**Acknowledgments**

I would like to thank Mr. Ted Kinsman, my physics teacher, for encouraging me to apply to this program and writing my recommendation for this program. I would like to thank Wolf Seka, Dustin Froula, and Steven Ivancic for helpful discussions. I would especially like to thank my adviser, Mr. Robert Boni, for all the help and time he gave me, as well as Dr. Stephen Craxton for running the program. I would also like to thank the Lab for Laser Energetics for supporting this high school program.

## References

1. W. Seka, C. Stoeckl, V. N. Goncharov, R. E. Bahr, T. C. Sangster, R. S. Craxton, J. A. Delettrez, A. V. Maximov, J. Myatt, A. Simon, and R. W. Short, *Absorption Measurements in Spherical Implosions on OMEGA*. Bull. Am. Phys. Soc., 49 179 (2004).
2. W. Seka, D. H. Edgell, J. P Knauer, J. F Myatt, A. V. Maximov, R. W. Short, T. C. Sangster, C. Stoeckl, R. E. Bahr, R. S. Craxton, J. A. Delettrez, V. N. Goncharov, I. V. Igumenschchev, and D. Shvarts, *Time-Resolved absorption in cryogenic and room-temperature direct drive implosions*. Physics of Plasmas, 15, 056312 (2008).
3. W. Seka, V. N. Goncharov, J. A. Delettrez, D. H. Edgell, I. V. Igumenschchev, R. W. Short, A. V. Maximov, J. Myatt, and R. S. Craxton, *Time-Dependent Absorption Measurements in Direct-Drive Spherical Implosions*. Phys. Rev A, 36, 3926 (1987).
4. Robert Boni, private communications.
5. Palmer, Christopher. *Diffraction Grating Handbook Fifth Edition*. 2002 Pg 17.
6. Photon Engineering website, <<http://www.photonengr.com/>> September 18, 2012.
7. W. Seka, D. H. Edgell, J. F Myatt, A. V. Maximov, R. W. Short, V. N. Goncharov, and H. A. Baldis, *Two-Plasmon-decay instability in direct-drive inertial confinement fusion experiments*. Physics of Plasmas, 16, 052701 (2009).
8. D. H. Froula, L. Divol, A.A. Offenburger, N. Meezan, T. Ao, G. Gregori, C. Niemann, D. Price, C.A. Smith, and S. H. Glenzer, *Direct Observation of the Saturation of Stimulated Brillouin Scattering by Ion-Trapping Induced Frequency Shifts*. Phys. Rev. Letters, 93, 035001